# Passive Axial Thrust Bearing for a Flywheel Energy Storage System

Magnus Hedlund, Johan Abrahamsson, Jesús José Pérez-Loya, Johan Lundin and Hans Bernhoff

Uppsala University, Division for Electricity, Uppsala, Sweden
Magnus.Hedlund@Angstrom.uu.se

**Abstract**

Two types of passive magnetic lift bearings are evaluated in terms of lift force and eddy current losses. Two sources of eddy currents are analyzed with help of the finite element method, firstly losses due to non-radial magnetization of magnets, and secondly losses due to variations in remanence. Magnets placed are placed in a Halbach array on the rotor and ring-magnets are placed on the stator. Denoted semi-segmented bearings, these produce low losses in the rotor, thus limiting the need of heat transport during vacuum operation. Experimental results of lift force are presented, together with simulations results. The losses were found to be in the order of 9 W at a rotational speed of 30 000 rpm while producing 900 N of thrust. The FEM-problem is solved with time-dependent terms, and is compared with a stationary approximation.

## 1 Introduction

A high-power electric flywheel for short-time energy storage in mobile applications, preferably with high power-to-energy ratio, is studied at the Division for Electricity at Uppsala University. The flywheel is part of a driveline, fully or partially electric depending on the main energy storage which may consist of a battery, a fuel cell or a diesel generator. A typical application would be a city bus with frequent stops or a construction machine alternating idling periods with heavy work. The flywheel has many purposes, of which the most important is to protect the main energy storage from transients, thus increasing its lifetime and significantly lower its power demands, enabling a higher energy density of the storage in return. The flywheel also enables efficient regenerative braking [1].

The rotor of the flywheel prototype built weighs 45 kg which gives a storage capacity of 800 Wh at its maximum rotational speed of 30 000 rpm [2, 3]. It consists of a combination of a high-end carbon fibre and a less expensive glass fibre rim to lower production costs. To minimize stand-by losses, the flywheel rotor is operated in near vacuum and suspended on magnetic bearings. The bearings are divided into passive thrust bearings formed by magnets operating in repulsive mode, and active electromagnets for radial positioning of the rotor.

### 1.1 Aim

This paper presents a simulated eddy current loss study, as well as lift force optimizations and measurements. Two types of bearings are analysed, here denoted as the fully segmented bearing and the semi-segmented bearing. Eddy current losses are simulated with of FEM, and specifically losses due to inhomogeneous fields are studied (losses due to gyroscopic effects are not included). Some comparisons between time-domain and stationary solutions are also presented. The semi-segmented bearing is optimized for high lift force. Eddy current losses in ring shaped magnets have been studied theoretically in [4] by application of Ampère's law.

Figure 1: Photo of the flywheel prototype currently being finalized at Uppsala University.

## 1.2 Bearings

The passive bearing utilizes magnets operating in repulsive mode, and is comprised of two units mounted on the rotor and stator respectively. No back-iron is used in these designs to minimize eddy-current losses. The fully segmented bearing concept involves segmented units (seen in Figure 2) on both rotor and stator; the semi-segmented bearing is comprised of a ring-magnet unit (seen in Figure 3) mounted on the stator, and a segmented unit on the rotor.

### 1.2.1 Fully segmented bearing

Three rows of magnets with different magnetization directions are placed to form a Halbach array [5], thus concentrating the field density on one side of each unit. The lift-force and a simple eddy-current analysis of this bearing were presented in [3]. The units can sustain high centrifugal loads since the magnets are free to expand radially. Under the assumption of perfect alignment, eddy currents inside the magnets (when one unit is rotating above the other) are induced due to a slight variation of the magnetic field around the circumference. These variations mainly arise due to:

- The radial magnets required to form a Halbach array cannot be magnetised truly radially during manufacturing.
- Small geometrical variations (not analysed here).
- The remanence of the each individual magnet might vary from batch to batch.

The manufacturer claims the remanence is between 1.35 - 1.40 T for the particular N48-grade neodymium magnets used. The conductivity for the NeDyFeB-magnets was assumed to be 6.9444 $MSm^{-1}$ and the relative permeability was assumed to be 1.05.

### 1.2.2 Semi-segmented bearing

The semi-segmented bearing has a segmented Halbach unit placed in the rotor, while the stator features a unit comprised of two ring-magnets as seen in Figure 3 (studied in [6] for a radial bearing). The ring-magnet unit is not mounted in a Halbach array (due to limitations in manufacturing) and the magnets are magnetized in only the axial direction, which implies a

Figure 2: A segmented unit, which constitutes one half of the segmented Halbach bearing. The inner row is magnetized inwards, the middle row radially outwards and the outer row outwards.

Figure 3: A ring-magnet unit, which constitutes one half of the Semi-segmented bearing, with magnetic fields directed inwards for the inner magnet. The opposite applies for the outer magnet.

lower attainable lift force per unit volume. The benefits of these units are that there are no variations in remanence due to differences between magnet manufacturing batches (since only one magnet per row is used), as well as no need for a radial magnetization, which completely removes the effect of non-radial field. Since these units are sensitive to radial expansion, they are mounted on the stator only, and the segmented units mounted on the rotor will still induce currents in the stator magnets. The rotor losses are expected to be lowered, but the stator losses are assumed to stay the same. Heat sources on rotors operating in vacuum are problematic, and the semi-segmented bearing concept minimizes this effect.

### 1.2.3 Semi-segmented isolated bearing

All the individual magnets mentioned above are covered in a thin layer of protective Ni & Cu-coating, which is conductive. The eddy currents can be limited in magnitude by isolating the magnets in the segmented units with an additional coating of varnish, which can be added during manufacturing. This has some positive implications to the free current density distributions inside the material. Heat transfer must be taken into account as varnish can decrease heat conductivity.

## 2 Method

The commercial FEM-solver COMSOL Multiphysics was used to evaluate lift force and eddy current losses in the magnetic bearing. All the simulations below are done with non-conductive stationary magnets on top, and a rotating conductive domain below which is not magnetized. The induced currents then appear in the conductive domain, so the losses for one bearing is a combination of two simulations; currents induced by the rotating unit inside the stationary and the opposite. The losses are thus defined from a unit (onto another unit).

The well-known Faraday's law, Ampère's law and the potential definitions are:

$$\nabla \times \mathbf{H} = \mathbf{J_f} + \frac{\partial \mathbf{D}}{\partial t} \tag{1}$$

$$\nabla \times \mathbf{E} = -\frac{\partial \mathbf{B}}{\partial t} \tag{2}$$

$$\mathbf{B} = \nabla \times \mathbf{A} \tag{3}$$

$$\mathbf{E} = -\nabla \phi \tag{4}$$

A first order polynomial is used for constitutive relation of the magnetization $\mathbf{M}$:

$$\mathbf{M} = \mathbf{B}_r + (\mu_r - 1)\mathbf{H} \tag{5}$$

Faraday's law and Eq. 3 gives:

$$\nabla \times \left( \mathbf{E} + \frac{\partial \mathbf{A}}{\partial t} \right) = 0 \tag{6}$$

Since $\nabla \times (\nabla u) = 0 \, \forall u$, the equation becomes (via Eq. 4):

$$\mathbf{E} = -\nabla \phi - \frac{\partial \mathbf{A}}{\partial t} \tag{7}$$

Given a moving observer in an inertial system (denoted with prime), a stationary magnetic field will induce an apparent electric field in the moving frame [7, Ch. 17-3]:

$$\mathbf{E}' = \mathbf{E} + \mathbf{v} \times \mathbf{B} \tag{8}$$

Assuming no other external sources of current, the current density can then be rewritten as:

$$\mathbf{J}_f = \mathbf{J}' = \sigma \mathbf{E}' = \sigma(\mathbf{E} + v \times \mathbf{B}) \tag{9}$$

Ampère's law can thus be rewritten with the help of Eqs. 3, 5, 7 and 9:

$$\nabla \times \left( \mu_0^{-1} \mathbf{B} - \mathbf{M} \right) = \nabla \times \left( \frac{\nabla \times \mathbf{A}}{\mu_0 \mu_r} - \mathbf{B}_r \right) = \sigma \left( -\nabla \phi - \frac{\partial \mathbf{A}}{\partial t} + \mathbf{v} \times (\nabla \times \mathbf{A}) \right) + \frac{\partial \mathbf{D}}{\partial t} \tag{10}$$

The displacement current is neglected due to the low frequencies involved, and by solving for $\mathbf{A}$, the equation simplifies to:

$$\nabla \times \left( \frac{\nabla \times \mathbf{A}}{\mu_0 \mu_r} - \mathbf{B}_r \right) + \sigma \frac{\partial \mathbf{A}}{\partial t} - \sigma \mathbf{v} \times (\nabla \times \mathbf{A}) = 0 \tag{11}$$

Equation 11 can be used to model moving conductive domains in the time-domain.

Non-conductive domains will not contain any free currents, thus reducing Ampère's law to its rotation-free form:

$$\nabla \times \mathbf{H} = \mathbf{J}_f = 0 \tag{12}$$

which enables the use of a scalar potential $\phi_m$:

$$\mathbf{H} = -\nabla \phi_m \tag{13}$$

By inserting Eq. 5 and 13 into Gauss' law for magnetism, a simpler equation is attained:

$$\nabla \cdot (\mathbf{B}_r - \mu_0 \mu_r \nabla \phi_m) = 0 \tag{14}$$

The velocity term is defined in a cylindrical system:

$$\mathbf{v} = 2\pi r f \hat{\varphi} \tag{15}$$

where $f$ is the rotational speed of the bearing.

## 2.1 Lift force

### 2.1.1 Simulation

The stationary scalar magnetic potential (Eq. 14) was solved for the lift force simulation, and the Maxwell stress tensor was used to compute the force.

### 2.1.2 Optimization

The segmented unit was optimized for lift force in [3], and the circular unit can be optimized in a similar manner. The segmented unit geometry is assumed to be given as well as some geometric properties for the circular unit, see Table 1. The outer and inner radius of the magnetic materials are assumed given, and the variable to be optimized is the radial length of the inner magnet (the outer magnet is defined by the inner magnet).

| *Property* | *Value* |
|---|---|
| Magnet height | 10 mm |
| Max outer radius | 50 mm |
| Min inner radius | 25 mm |
| Inner magnet radius | Optimization variable |

Table 1: Geometrical properties of ring-magnet unit

Under these constraints the optimization problem has only one degree of freedom, and the maximum force is easily found by FEM. The airgap was chosen to 5 mm during optimization.

### 2.1.3 Experimental measurement

A semi-segmented bearing was constructed and mounted in a stationary setup for evaluation of standstill lift-force.

## 2.2 Time-dependent eddy current loss simulation

A time-dependent magnetic simulation of the bearing is performed. The moving, conductive magnets are modeled with Eq. 11, while the surrounding air and the stationary, non-conductive magnets are modeled with Eq. 14 to reduce complexity. The differential equations are coupled via a mixed formulation boundary conditions (provided by Comsol).

### 2.2.1 Loss computation

The total electromagnetic losses are computed as an integral over one revolution of momentary electromagnetic loss. The momentary losses are computed as [7, Ch. 12-4]:

$$P_{loss,momentary}(t) = \int_{Volume} \bar{J}_{free}(t) \cdot \bar{E}(t) dV \tag{16}$$

which in turn yields to the total loss expression:

$$P_{loss} = f \int_{t=0}^{t=1/f} P_{loss,momentary}(t)dt \tag{17}$$

### 2.3 Stationary loss simulation - velocity term

An approximation of the time-dependent solution is to neglect $\frac{\partial \mathbf{A}}{\partial t}$, which, if applied to Eq. 11, yields the following equation:.

$$\nabla \times \left( \frac{\nabla \times \mathbf{A}}{\mu_0 \mu_r} - \mathbf{B}_r \right) - \sigma \mathbf{v} \times (\nabla \times \mathbf{A}) = 0 \tag{18}$$

This approximation is simpler than a full time-dependent solution since it does not require computation of intermediate steps. The differential equation above is an approximation if applied for a rotating device in which geometry, material properties or magnetic sources ($\nabla \cdot \bar{M}$) are not constant in the circumferential direction (in a cylindrical coordinate system with its z-axis on the rotational axis). FEM-tools such as Comsol readily supports this quasi-static system formulation.

The stationary formulation is less computationally demanding than the time-domain approach described above, but is expected to be less accurate since it doesn't incorporate self-inductive effects. A simplified geometry, seen in Figure 12, is used to compare eddy current losses between stationary and time-dependent simulations.

## 3 Results

### 3.1 Lift Force

The lift-force for the semi-segmented bearing was computed for every different value of the optimization variable, with results seen in Figures 4 and 5. A maximum lift force is attained for a radial length of 14 mm for the inner magnet, and consequently the outer magnet is set at 11 mm. The semi-segmented bearing was experimentally verified and the results are presented in Figure 6 along with a comparison of the lift-force from a fully segmented bearing (which was verified experimentally in [3].

### 3.2 Stationary loss simulation - velocity term

#### 3.2.1 Non-radial magnetization

The losses due to non-radial magnetization were computed for fully segmented and semi-segmented units as well as for non-isolated units as seen in Figures 7 and 8 respectively.

#### 3.2.2 Remanence variation

The remanence variations were found to be small, so the meshing had to be done with care to avoid unnecessary artefacts.

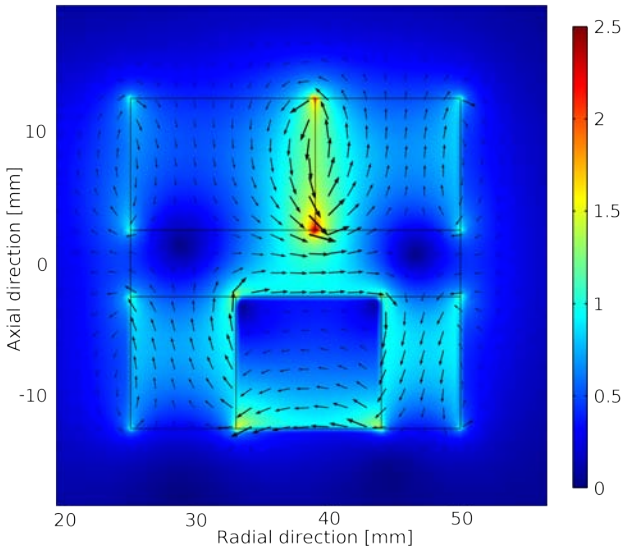


Figure 4: A radial-axial cutaway view of the magnetic flux density (in T) at an airgap of 5 mm in the semi-segmented bearing with a ring-magnet unit on top and a segmented unit below.

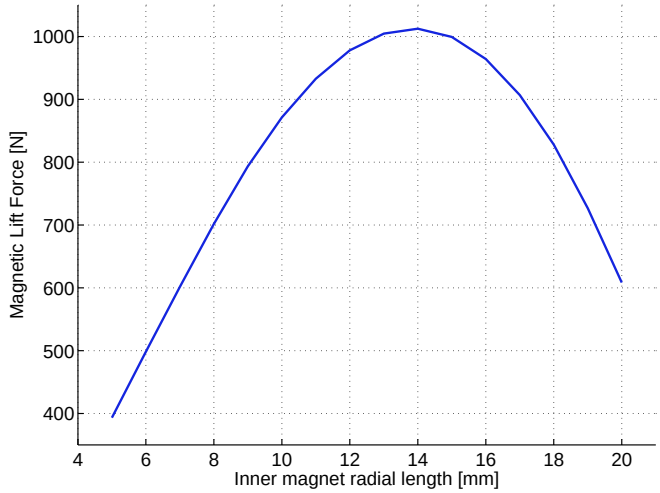


Figure 5: Simulated lift force as a function of radial length of the inner magnet, with a maximum at 14 mm.

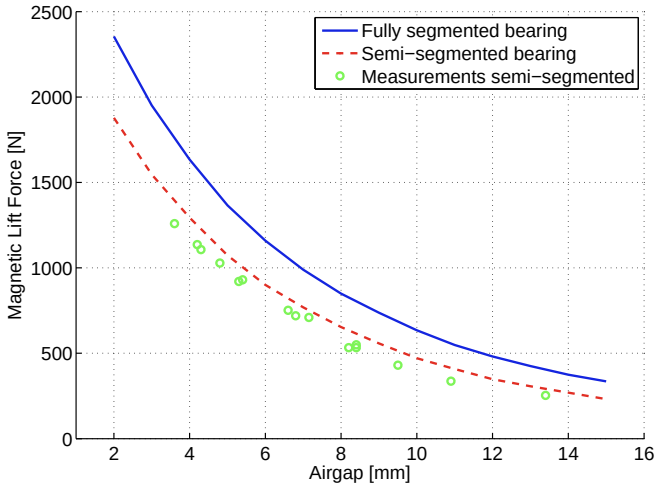


Figure 6: A semi-segmented bearing features about 75% relative lift force compared to the fully segmented concept.

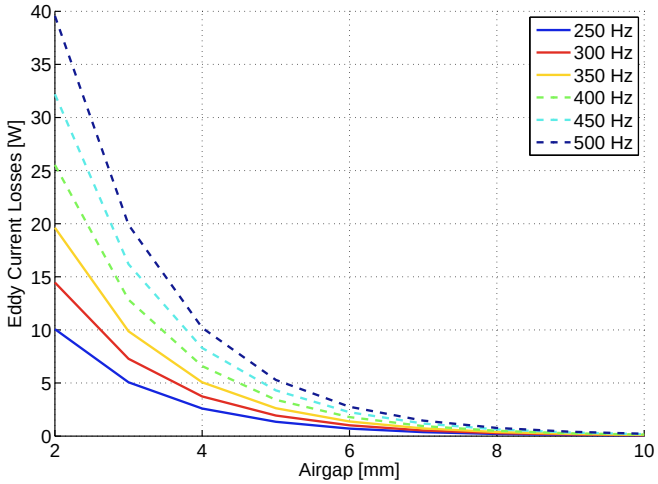


Figure 7: The frequency dependency of the eddy current losses due to nonradial magnetization in the fully segmented non-isolated bearing. The semi-segmented non-isolated bearing features about 50% of these losses.

**Meshing** A tetrahedal mesh did not produce any usable results at all, the solution contained unwanted induced currents in locations with a uniform magnetic field even though a high number of mesh elements were used. The ratio of induced currents contra mesh artefacts was relatively poor, only 5:1. A hexahedral mesh produced much less of these mesh-induced currents for the same amount of elements, but artefacts were still visible as seen in Figure 9. Further mesh refinement led to an induced currents contra artefacts ratio of 50:1, which was found to be an acceptable trade-off between computational time and accuracy. The number of mesh elements were tripled during this process.

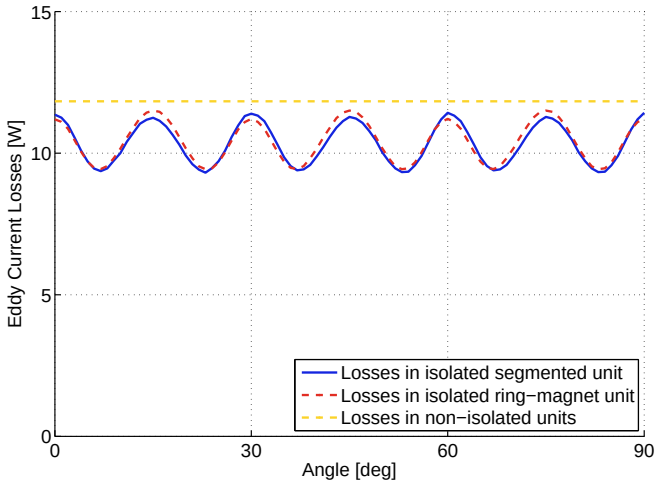


Figure 8: Stationary losses for the three different bearing units.

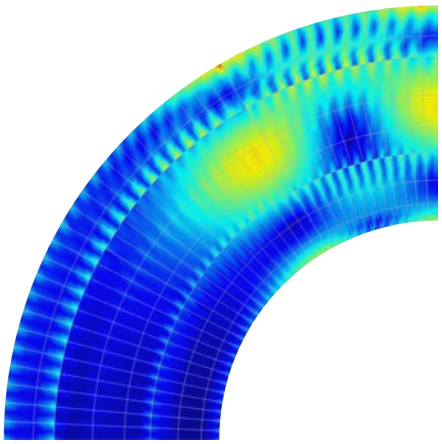

Figure 9: Artefacts in the induced current data when using a hexahedral mesh (drawn in grey). One magnet in the upper part of the figure is overmagnetized and should be the only source of varying magnetic field in this simulation, but there are small induced currents spread evenly around the circumference. The expected induced currents to artefacts ratio of this simulation is 19:1.

Note that these artefacts only appeared when applying a radial magnetization to a domain, the non-radial magnetization solution above did not suffer from these artefacts. The artefacts are probably an effect of discrete magnetization in single mesh points, causing a variation around the circumference which is suppressed when increasing total number of mesh points.

**Losses** As seen in Figure 10, the losses due to remanence variations are substantially lower than those associated with a non-radial magnetization. Half of the magnets were magnetized to 1.35 T, and the other (radially distributed) triplets of magnets were all magnetized to some value between 1.35 T and 1.40 T. When traversing the circumference, each variation in magnetization

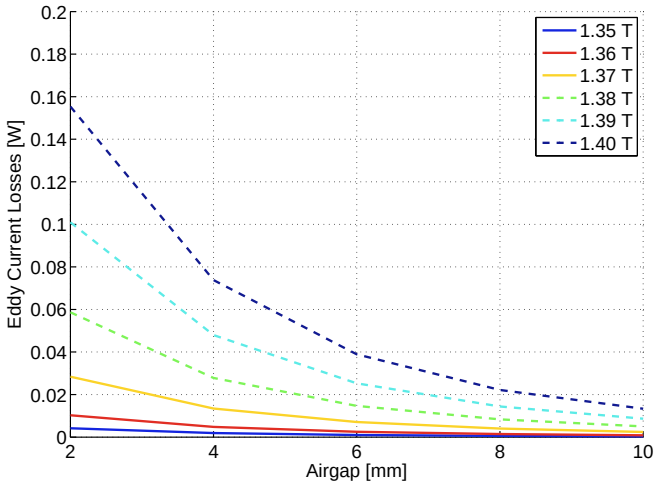


Figure 10: Losses in bearing when every magnet but one radial triplet is magnetized to 1.35 T. The differing triplet is magnetized as in the figure legend.

results in some losses (the simulation in the figure is a result of one of these transitions). The resulting bearing loss is a combination of every transition, and is thus dependent on some remanence distribution function. A worst case scenario can be constructed (assuming magnet remanence is confined to an interval $B_r \in [1.35, 1.40]$) if every other magnet triplet is chosen to be the minimum and the maximum respectively. The worst case $\Delta B_r$-losses for one segmented unit at an nominal airgap of 6 mm at 500 Hz then becomes $P_{worst} = 0.48W$.

## 3.3 Time-dependent eddy current loss simulation

The time-dependent solution was found to be quite computationally demanding compared to the stationary loss-simulation due to the need of many intermediate time-steps.

### 3.3.1 Non-radial magnetization

Time-dependent solutions for the non-radial magnetization of segmented units led to losses lower than for the stationary case. Figure 11 shows losses for a unit rotating above a segmented unit, with identical results for ring-magnet units and segmented units. The total bearing loss differs by a factor of two, since the segmented units do not induce currents in the segmented bearing due to this effect.

### 3.3.2 Remanence variation

The remanence variations were too small to distinguish by time-dependent simulation, due to requirements on the mesh as discussed in 3.2.2. A simplified test case with a larger step in remanence (from 0 to 1.35 T) was used to compare how the different methods handled variations in magnetization intensity. These two produced similar results, as can be seen in Figure 13. The geometry of the model can be seen in Figure 12.

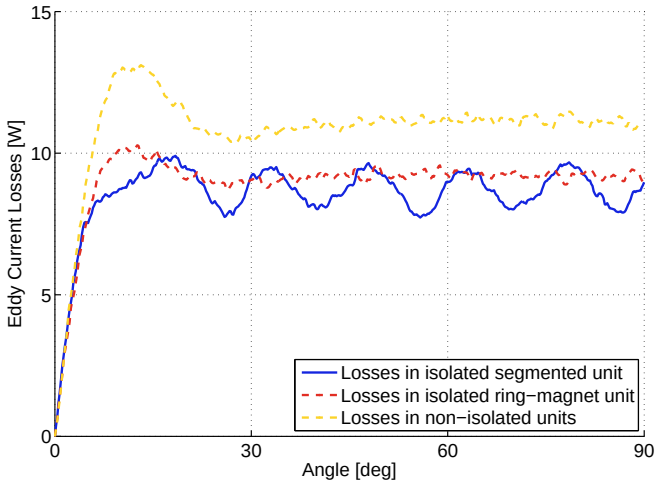


Figure 11: The time-dependent eddy current losses are computed for a rotational velocity of 500 Hz at the nominal air gap of 6 mm. The time-dependent solver estimated losses lower than the stationary solver.

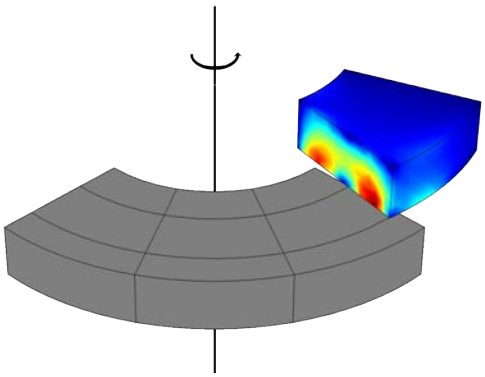

Figure 12: Geometry for the simplified time-dependent simulation. One conductive magnet-triplet is flying past three other magnet-triplets. The induced current density is drawn on the moving magnets' surface. The magnetic field variation in this particular problem is large compared to computational errors, which simplifies comparison of the time-domain and stationary loss calculation approaches.

## 3.4 Remarks

The semi-segmented bearing itself is not optimized for lift force, here the ring-magnet unit is optimized given one segmented unit from an optimized fully segmented bearing. At this stage in the project the investment in lift-bearing magnets had already been done.

Isolated magnets are simulated one by one, the influence from eddy currents in magnet to its neighbour is thus not modeled here.

In [3], the magnitude of the losses are estimated by the stationary velocity term described above, although at only one angle. Also, the conductivity used in this article is half the value

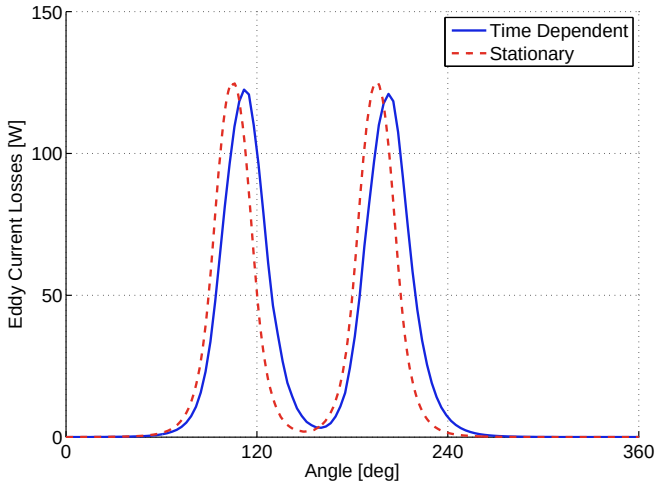


Figure 13: The time-dependent and the stationary solution are similar in magnitude. The magnet was rotating at 500 Hz for the given solution. The mean relative loss power difference is 13%. Self-inductance in the eddy-currents are assumed to be the cause of the larger area below the time-dependent peak seen in the graph above. The stationary solution provided the highest peak value.

used there.

# 4 Conclusion

The losses were found to be low for the semi-segmented magnetic bearing, and a perfectly centered semi-segmented unit mounted on the stator does not produce any of the studied losses in the rotor, which is good for requirements of the flywheel application. The losses in the stator was found to be in the order of 9 W at 30 000 rpm at nominal airgap of 6 mm. Losses in fully segmented units were twice this, around 18 W.

Two eddy current sources were studied, firstly induction due to non-radial magnetization of the middle magnets in the segmented units and secondly induction due to manufacturing variations in magnetic remanence. These two effects were isolated into different simulations, and the non-radial magnetization was estimated to induce more than 10 times more losses than remanence variations.

# References

[1] Johan Lundin. *Flywheel in an all-electric propulsion system.* Licenciate thesis, Uppsala Universitet, Uppsala, Sweden, 2011.

[2] Johan Abrahamsson, Magnus Hedlund, Tobias Kamf, and Hans Bernhoff. High-speed kinetic energy buffer: Optimization of composite shell and magnetic bearings. *IEEE Transactions on Industrial Electronics*, 2013, 2013. Accepted, not yet published.

[3] Johan Abrahamsson, Magnus Hedlund, and Hans Bernhoff. Kinetic energy storage for vehicular applications. In *13th International Symposium on Magnetic Bearings*, Virginia, USA, 2012.

[4] Olivier Bouty. Eddy current losses in passive magnetic bearings. *Journal of Applied Physics*, 92(11):6851–6856, 2002.

[5] Z.Q. Zhu and D. Howe. Halbach permanent magnet machines and applications: a review. *Electric Power Applications, IEE Proceedings* -, 148(4):299–308, 2001.

[6] J.-P. Yonnet, G. Lemarquand, Sophie Hemmerlin, and Elisabeth OlivierRulliere. Stacked structures of passive magnetic bearings. *Journal of Applied Physics*, 70(10):6633–6635, 1991.

[7] Roald K. Wangsness. *Electromagnetic fields*. Wiley, July 1986.